# Simulated Corrosion Product Deposition Experiment on Zirconium Fuel Cladding in PWR primary water condition for Evaluating Thermal Properties

Junhyuk Jeong, Yunju Lee, Ji Yong Kim, In Cheol Bang and Ji Hyun Kim*

*Department of Nuclear Engineering, College of Engineering,*
*Ulsan National Institute of Science and Technology (UNIST)*
**Corresponding author: kimjh@unist.ac.kr*

## 1. Introduction

To enhance the operational economy and to reduce waste in NPP(Nuclear Power Plants), the utilization of high burnup nuclear fuel (about 60MWd/kg) is on the rise. Under high burnup conditions, the nuclear fuel cladding is exposed to harsh environments, leading to material degradation issues. Particularly, the formation of oxide layers on cladding surfaces and CRUD (Chalk River Unidentified Deposit) deposition, induced by power increase and operational cycles, can change the neutron transfer and thermohydraulic behavior near fuel rods inducing economic and safety problems.[1]

CRUD is composed of corrosion products like Nickel ferrite, NiO, $Fe_3O_4$, or $Ni_2FeBO_5$. These particles are formed in structural materials like steam generator and stainless steel tubes and carried into the core through primary coolant.[2] The corrosion products particles are accumulate on fuel cladding forming porous CRUD. CRUD not only affects neutron transport behavior on the fuel rod surface by absorbing boron from the coolant, leading to phenomena like AOA (Axial Offset Anomaly) or CIPS(CRUD Induced Power Shift), but also increases thermal resistance on the cladding surface, accelerating localized corrosion known as CILC (CRUD Induced Localized Corrosion) due to elevated cladding temperatures.[1,2]

To predict and prevent those problems, it is essential to understand the deposition behavior and acquire data on the morphology and properties of CRUD under various environmental conditions. In this study, using the DISNY (crud DeposItion Simulator for Nuclear energY) [3], which simulates PWR primary coolant conditions, we investigate the structural changes of CRUD deposition under various environmental parameters such as coolant flow rate, cladding surface heat flux, and CRUD deposition time.

In this paper, the effect of coolant flow rate on fuel CRUD formation was investigated through CRUD deposition experiments conducted under three different flow rate conditions. The specimens are then analyzed using SEM-EDS to characterize their structural and chemical properties.

## 2. Experimental Methods

### *2.1. Experimental condition and facility*

CRUD deposition experiment was conducted to investigate the characteristic of CRUD according to the thermohydraulic condition and water chemistry condition. Three major conditions should be satisfied for CRUD deposition, sub-cooled boiling at cladding surface, existence of corrosion product in the primary water, and boron and lithium ion in the primary water. Because the CRUD deposition behavior occurs at upper span of the fuel assembly, the experimental conditions was set to simulate the top span of fuel assembly of OPR1000. (Table 1) 300 mm of Zr-Nb-Sn alloy tube is used for fuel cladding specimen. Using direct current heating method, heat flux condition on surface of the specimen was satisfied.

**Table 1** Reference condition of CRUD deposition experiment in DISNY.

| Experimental conditions | Reference condition |
|---|---|
| **Exposure Time [hr]** | 36 |
| **Average heat flux [kW/m$^2$]** | 600 |
| **Average Flow Rate [kg/m$^2$-s]** | 1.07 |
| **Average Pressure [bar]** | 155.5 |
| **Average Bulk Temperature [°C]** | 333 |
| **DH concentration [mol/kg]** | 2.4 |
| **DO concentration [ppb]** | <5 |
| **B concentration [ppm]** | 1200 |
| **Li concentration [ppm]** | 2.2 |

Each experimental condition conducted was named in the format of Txx - Qxxx - Gxxxx, considering deposition time (T), crud deposition heat flux (Q), and mass flow rate (G). The T36-Q600-G3500 experiment was designated as the reference specimen, representing CRUD deposition under typical operational conditions.

To investigate the effect of coolant flow rate on CRUD morphology and properties, CRUD deposition experiments were conducted at two more different mass flux conditions, The T36-Q600-G1750 and The T36-Q600-G2450, and the results are detailed in Table 2.

**Table 2** Major experimental conditions of CRUD deposition experiments with different flow rate.

| | PZR-P [bar] | TX-$T_{in}$ [°C] | PRS G [kg/m$^2$s] | Dep. q“ [kW/m$^2$] | Dep. time [hr] |
|---|---|---|---|---|---|
| **T36-Q600-G3500** | 155.8 | 338.1 | 3,451.4 | 614.8 | 36.1 |

| | | | | | |
|---|---|---|---|---|---|
| **T36-Q600-G2450** | 155.3 | 336.4 | 2,333.3 | 617.2 | 36.0 |
| **T36-Q600-G1750** | 155.3 | 336.0 | 1,782.4 | 613.6 | 36.0 |

The corrosion product dissolved in primary water, is simulated by metal ions such as nickel and iron, which are injected with nickel acetate and Fe Ethylenediaminetetraacetic acid (EDTA). The proper Ni and Fe ion concentrations were assumed to be 325 and 160 ppb, respectively because in the NPP, which have severe CRUD deposition, the Ni and Fe ion concentrations of coolant exceed 200 ~ 300 ppb [3]. To accelerate the CRUD deposition, concentrated metal ion solutions were prepared to simulate one cycle (18 months) of NPP operation in the 36 hours of the experiment.

The CRUD experimental facility, DISNY is comprised of two loop part; water chemistry loop and test section loop. Coolant chemistry, such as the dissolved oxygen (DO) concentration, dissolved hydrogen (DH) concentration, pH, boron concentration, and lithium concentration, is controlled in the water chemistry loop and flows into the test section loop where high-pressure, high-temperature, and high-flow conditions was established. For the in-situ surface temperature measurement, a thermocouple was installed in the cladding specimen, contacting the inner surface, as described in Figure 1.

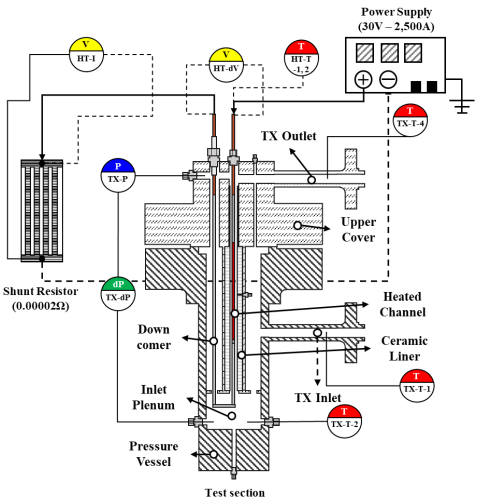


**Figure 1** Schematic diagram of DISNY CRUD simulation loop facility.

*2.2. Analysis strategy*

After completing the experiments, we sectioned 300 mm cladding specimens with CRUD deposition into four samples, as shown in Figure 2, for structure analysis. In this paper, we compare 160mm - 200mm region of each specimen. Structural characteristics of CRUD, expected to influence its thermal properties, was analyzed. Also, quantitative characterization was conducted focusing on morphological and chemical structural aspects. This included determining CRUD layer thickness, measuring CRUD nuclei diameter and porosity, and quantifying chemical composition, such as the Ni, Fe and O content.

Using FIB (Focused Ion Beam) equipment integrated with a SEM (Scanning Electron Microscope), surface and cross-sectional images of the CRUD deposition specimens were obtained. Subsequently, the images were rigorously analyzed to precisely quantify CRUD thickness, porosity, density, and chimney diameter.

For compositional analysis of CRUD, we employed SEM-EDS (Energy Dispersive X-ray Spectroscopy) to examine the surface or cross-sections of the CRUD.

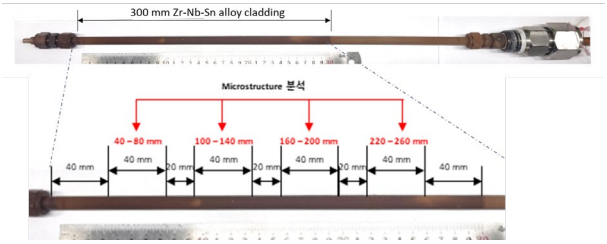


**Figure 2** Example of CRUD specimen sectioning.

## 3. Results and discussion

*3.1. Morphology and chemistry of reference specimen (T36-Q600-G3500)*

Microstructure of CRUD layer in reference specimen T36-Q600-G3500, were characterized, focusing solely on regions close to the inner wall temperature measurement locations. The results were compared with analyses of CRUD deposited on nuclear fuel cladding in NPP [4], to confirm the successful simulation of CRUD deposition in DISNY.

By analyzing SEM images of the CRUD deposition specimen surfaces, we derived data on CRUD chimney characteristics on the reference specimen's surface. The majority of particles observed were amorphous, with a significant amount of agglomerated particles observed in the 160mm to 200mm region. The chimney structure was most prominent at inner layer and became denser towards the outer layer, with decreasing particle diameters and increasing density.

We also obtained SEM images of CRUD layer cross-sections by ion beam processing a single spot on the surface of the CRUD deposition specimens. These images revealed that the CRUD layer comprised two distinct layers with differing particle shapes and densities, designated as the inner and outer layers. The inner layer mainly consisted of amorphous particles, while the outer layer comprised densely packed amorphous particles, with some agglomerated particles observed, particularly in the region of 160mm to 200mm.

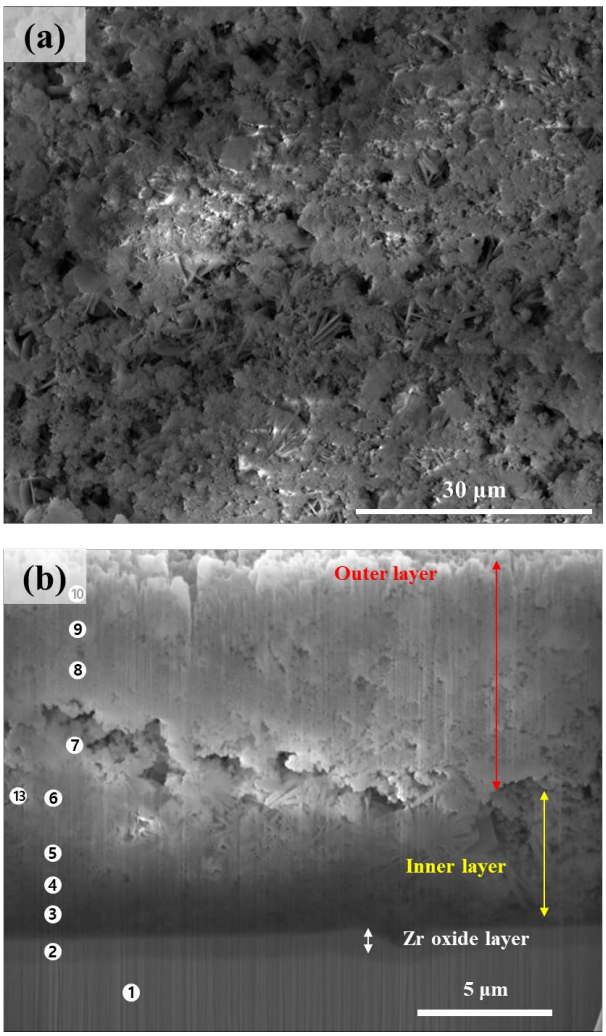


**Figure 3** Surface and cross sectional SEM images of CRUD layer in 160 mm ~200 mm region of T36-600-G2450 specimen (reference specimen)

**Table 3** Chemical composition of T36-Q600-G3500(reference specimen) measured by EDS**.**

| | # | O [at.%] | Zr [at.%] | Fe [at.%] | Ni [at.%] | Ni/Fe |
|---|---|---|---|---|---|---|
| **Zr** | 1 | 38.76 | 34.77 | 9.95 | 16.52 | 1.66 |
| **Zr oxide** | 2 | 44.79 | 50.80 | 1.35 | 3.06 | 2.26 |
| **Inner CRUD layer** | 3 | 65.46 | 10.98 | 1.26 | 22.31 | 17.70 |
| | 4 | 67.38 | 5.42 | 1.99 | 25.21 | 12.67 |
| | 5 | 64.80 | 4.20 | 3.17 | 27.82 | 8.78 |
| | 6 | 68.37 | 4.19 | 3.95 | 23.49 | 5.95 |
| | 7 | 68.91 | 2.63 | 4.70 | 23.76 | 5.06 |
| **Outer CRUD layer** | 8 | 57.10 | 4.41 | 17.23 | 21.26 | 1.23 |
| | 9 | 59.47 | 3.17 | 16.49 | 20.87 | 1.27 |
| | 10 | 67.68 | 1.77 | 13.32 | 17.23 | 1.29 |

Utilizing energy-dispersive X-ray spectroscopy (EDS), we analyzed the chemical compositions of CRUD inner and outer layers at various positions along the cladding length. The Ni/Fe ratios obtained allowed us to calculate the ratios of NiO and NiFe2O4 deposition within the CRUD. Across all specimens, Ni/Fe ratios exceeded 0.5, indicating deposition of both NiO and NiFe2O4. Notably, the inner layer of the reference specimen at 160mm to 200mm exhibited the highest Ni/Fe ratio, indicating a predominance of NiFe2O4. This suggests that the presence of agglomerated NiO particles significantly increases the Ni/Fe ratio near the CRUD/cladding interface.

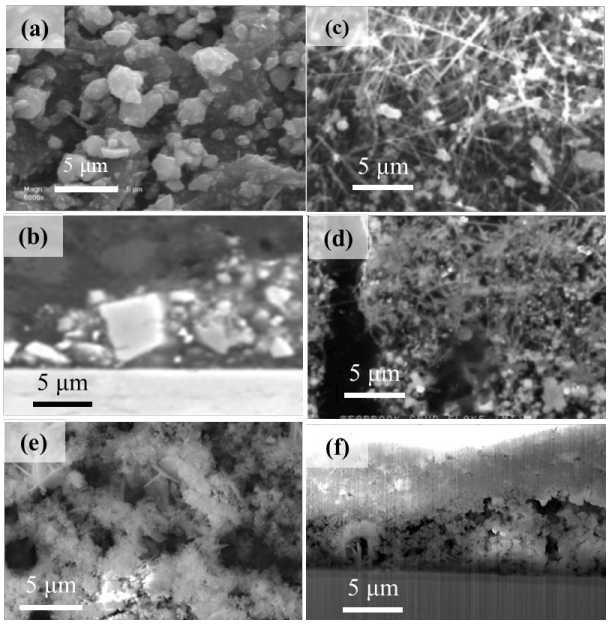


**Figure 4** Surface and cross sectional SEM image of CRUD layer deposited on fuel cladding in (a), (b) Uljin [4], (c), (d) Seabrook [5], (e), (f) DISNY reference specimen.

Furthermore, we evaluated the CRUD analysis results of the reference specimen T36-Q600-G3500 by comparing them with analyses of CRUD deposited in actual nuclear power plants. Due to limited availability of operational data from power plants and variations in environmental conditions, direct comparison was challenging. However, qualitative comparisons were made with analysis cases from Uljin Unit 3 [4], where no axially oriented accumulation (AOA) occurred, and Seabrook Cycle 5, where significant AOA and thick CRUD deposition were observed. The results of the reference specimen's CRUD closely resembled those from Seabrook, suggesting that the experimental conditions effectively simulated high-concentration metal ion conditions, similar to those at Seabrook[5].

Thus, comparing CRUD deposition from nuclear power plants with our experimental results, we find that DISNY experiments can adequately simulate CRUD deposition on pressurized water reactor fuel cladding, particularly resembling conditions observed at Seabrook NPP.

*3.2 Morphology and chemistry of specimen with different flow rates (T36-Q600-G1750 and T36-Q600-G2450)*

The experiments conducted at different flow rates (T36-Q600-G2450 and T36-Q600-G1750) both exhibited the formation of CRUD chimney structures, with T36-Q600-G1750 showing a particularly distinct chimney structure. In both experimental specimens, the CRUD outer layer exhibited densely packed amorphous particles, similar to the reference specimen. For T36-Q600-G2450, the presence of CRUD outer layer particles obscured the chimney structures, necessitating analysis of structural characteristics such as chimney diameter and density in areas where the outer layer was partially peeled off.

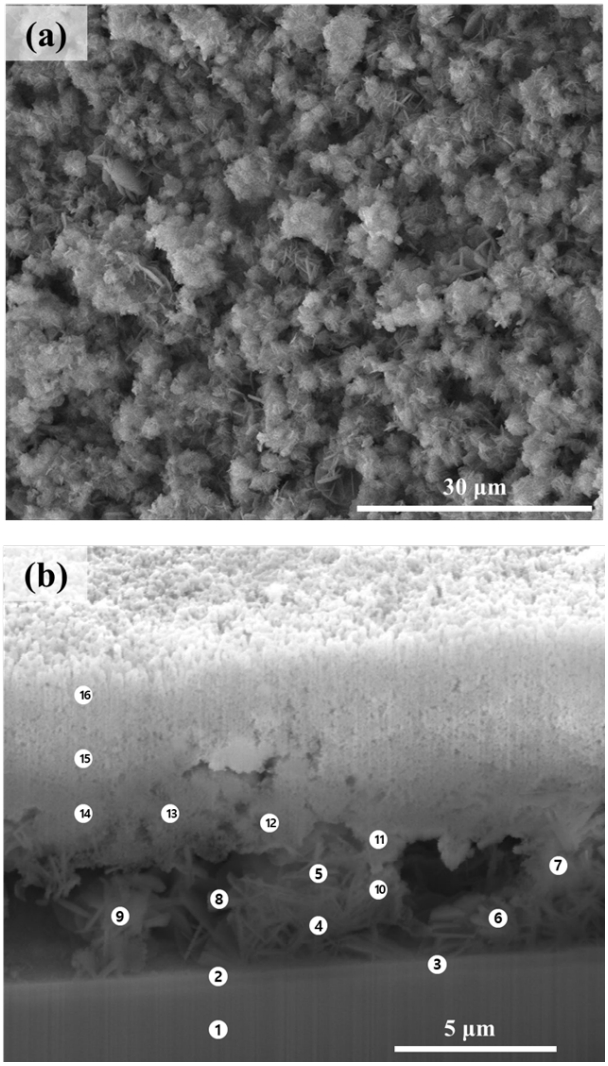


**Figure 5** Surface and cross sectional SEM images of CRUD layer in 160 mm ~200 mm region of T36-600-G2450 specimen

**Table 4** Chemical composition of CRUD layer in 160 mm ~200 mm region of T36-Q600-G2450 measured by EDS.

| | # | O [at.%] | Zr [at.%] | Fe [at.%] | Ni [at.%] | Ni/Fe |
|---|---|---|---|---|---|---|
| **Zr** | 1 | 27.05 | 67.19 | | | |
| **Zr oxide** | 2 | 48.98 | 45.02 | | | |
| | 3 | 46.45 | 29.76 | | | |
| **Inner CRUD layer** | 4 | 53.01 | 11.53 | 3.53 | 31.93 | 9.04 |
| | 5 | 55.04 | 5.09 | 5.83 | 34.04 | 5.84 |
| | 6 | 17.86 | 10.86 | 16.94 | 54.34 | 3.21 |
| | 7 | 14.73 | 7.75 | 10.50 | 67.03 | 6.38 |
| | 8 | 59.12 | 14.60 | 4.08 | 22.20 | 5.45 |
| | 9 | 63.03 | 11.82 | 4.13 | 21.01 | 5.09 |
| | 10 | 42.76 | 6.79 | 6.61 | 43.83 | 6.63 |
| | 11 | 33.37 | 6.55 | 15.82 | 44.26 | 2.80 |
| **Outer CRUD layer** | 12 | 48.79 | 6.68 | 15.87 | 28.66 | 1.81 |
| | 13 | 51.09 | 7.30 | 18.22 | 23.39 | 1.28 |
| | 14 | 50.82 | 9.83 | 15.94 | 23.41 | 1.47 |
| | 15 | 49.07 | 5.71 | 21.94 | 23.27 | 1.06 |
| | 16 | 58.92 | 3.08 | 17.67 | 20.33 | 1.15 |

Chimney density increased with flow rate, while chimney diameter decreased. The chimney area as a percentage of the total area decreased slightly with increasing flow rate, with 14% for T36-Q600-G1750 and 8% for T36-Q600-G2450. Average CRUD thickness measured from cross-sectional analysis increased with flow rate, with T36-Q600-G3500 exhibiting the thickest average Zr oxide thickness due to its higher flow rate.

Despite the anticipated decrease in CRUD deposition with increasing flow rate due to increased turbulent kinetic energy from higher flow rates not significantly increasing coolant temperature differences, CRUD deposition actually increased with flow rate. This is attributed to the increased mass flux of metal ions with higher flow rates.

Cross-sectional analysis revealed cubic particles in T36-Q600-G3500, sand-shaped particles in T36-Q600-G2450, and petal-like structures in T36-Q600-G1750, indicating structurally different forms due to erosion caused by flow rate differences and differences in metal ion quantities per unit time. The Ni/Fe ratio was approximately 5 to 6 in all three specimens, indicating predominantly NiO formation.

T36-Q600-G3500 and T36-Q600-G2450 exhibited approximately 30% porosity, confirmed by cross-sectional images obtained through scanning electron microscopy, revealing significant pores. T36-Q600-G1750 had a lower porosity of 18.5%, with smaller pores

observed between petal-like structures rather than large pores as seen in the other specimens.

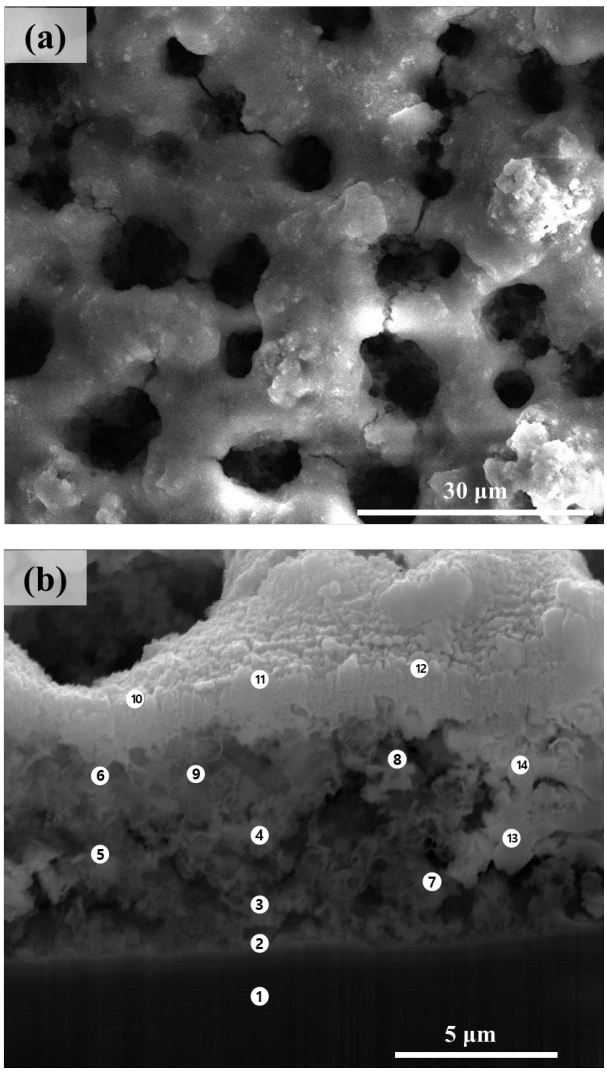


**Figure 6** Surface and cross sectional SEM images of CRUD layer in 160 mm ~200 mm region of T36-600-G1750 specimen

**Table 5** Chemical composition of CRUD layer in 160 mm ~200 mm region of T36-Q600-G1750 measured by EDS.

| | # | O(at.%) | Zr(at.%) | Fe(at.%) | Ni(at.%) | Ni/Fe |
|---|---|---|---|---|---|---|
| **Zr** | 1 | 27.05 | 67.19 | 2.25 | 3.51 | |
| **Zr oxide** | 2 | 48.98 | 45.02 | 2.20 | 3.80 | |
| **Inner CRUD layer** | 3 | 46.45 | 29.76 | 7.35 | 16.45 | 2.24 |
| | 4 | 53.01 | 11.53 | 3.53 | 31.93 | 9.04 |
| | 5 | 55.04 | 5.09 | 5.83 | 34.04 | 5.84 |
| | 6 | 17.86 | 10.86 | 16.94 | 54.34 | 3.21 |
| | 7 | 14.73 | 7.75 | 10.50 | 67.03 | 6.38 |
| | 8 | 59.12 | 14.60 | 4.08 | 22.20 | 6.63 |
| | 9 | 63.03 | 11.82 | 4.13 | 21.01 | 2.80 |
| **Outer CRUD layer** | 10 | 42.76 | 6.79 | 6.61 | 43.83 | 1.81 |
| | 11 | 33.37 | 6.55 | 15.82 | 44.26 | 1.28 |
| | 12 | 48.79 | 6.68 | 15.87 | 28.66 | 1.47 |

### *3.3. Effect of coolant flow rate on CRUD deposition*

The study investigated the effect of coolant flow rate on CRUD deposition, examining specimens T36-Q600-G2450 and T36-Q600-G1750 alongside the reference specimen T36-Q600-G3500. Structural and chemical characteristics of CRUD layer of each specimen were summarized in Table 6. All specimens exhibited CRUD chimney structures, albeit with varying characteristics. CRUD deposition increased with higher flow rates, contrary to anticipated reductions due to increased turbulent kinetic energy. This suggests that factors beyond flow dynamics, such as mass flux of metal ions, play significant roles in CRUD formation. Additionally, differences in CRUD morphology were observed among specimens, indicating varying erosion patterns and metal ion deposition rates.

Furthermore, variations in chimney density, particle shape, and porosity were noted across specimens. These differences underline the influence of flow rate on CRUD characteristics, with higher flow rates associated with denser chimney structures and increased porosity.

**Table 6** Structural and chemical characteristics of CRUD layer deposited on Zr fuel cladding

| Specimen | Axial position [cm] | Average thickness of Zr oxide layer [µm] | Average thickness of inner CRUD layer [µm] | Average thickness of outer CRUD layer [µm] | Chimney number density [#/m$^2$] | Average chimney diameter [µm] | Areal porosity of CRUD media [%] | Chemical composition of CRUD layer | | | | |
|---|---|---|---|---|---|---|---|---|---|---|---|---|
| | | | | | | | | Ni [at.%] | Fe [at.%] | O [at.%] | Ni/Fe ratio | NiO/$NiFe_2O_4$ |
| T36-Q600-G1750 | 18 | 0.6 | 4.96 | 7.91 | 3.07E+10 | 1.82 | 28.7 | 39.8 | 9.0 | 40.9 | 4.43 | 7.86 |
| T36-Q600-G2450 | 18 | 0.87 | 8.52 | 2.92 | 6.20E+09 | 5.43 | 18.5 | 41.7 | 9.5 | 37.6 | 5.78 | 10.56 |
| T36-Q600-G3500 | 18 | 1.2 | 8.88 | 9.25 | 2.23E+10 | 2.05 | 26.7 | 20.6 | 9.8 | 59.1 | 2.42 | 3.84 |

## 4. Conclusions

The effect of coolant flow rate on fuel CRUD formation was investigated through CRUD deposition experiments conducted under three different flow rate conditions using DISNY loop facilities. CRUD deposition increased with higher flow rates, contrary to anticipated reductions due to increased turbulent kinetic energy. This suggests that factors beyond flow dynamics, such as mass flux of metal ions, play significant roles in CRUD formation

## ACKNOWLDEGEMENT

This work was supported by the Nuclear Safety Research Program through the Korea Foundation of Nuclear Safety (KoFONS) using the financial resource granted by the Nuclear Safety and Security Commission (NSSC) of the Republic of Korea. (No. 2106022).

## REFERENCES

[1] Electric Power Research Institute. Report, Simulated Fuel Crud Thermal Conductivity Measurements Under Pressurized Water Reactor Conditions, TR-1022896, EPRI, Palo Alto, CA.
[2] Electric Power Research Institute. Report, PWR Axial Offset Anomaly (AOA) Guidelines, TR-1008102, EPRI, Palo Alto, CA.
[3] J.Y. Kim, Y. Lee, J. H. Kim and I. C. Bang, The DISNY facility for sub-cooled flow boiling performance analysis of CRUD deposited zirconium alloy cladding under pressurized water reactor condition: Design, construction, and operation, Nuclear Engineering and Technology, Vol.55, 2023, 3164-3182.
[4] Korea Atomic Energy Research Institute. Report, Control of Crud and Boron Deposition for AOA Prevention, KAERI/RR-3184/2009, ROK, Daejeon, 2009.
[5] Electric Power Research Institute. Report, Evaluation of fuel clad corrosion product deposits and circulating corrosion products in pressurized water reactors TR- 1009951, Palo Alto, California, 2004